Research Paper

Correction of Evanescent Wave Influence on the Flexural Wave Velocity and Wavelength Estimation Based on a Mode Shape Function

Filip PANTELIĆ(1)*, Dragana ŠUMARAC PAVLOVIĆ(2), Miomir MIJIĆ(2), Daniel RIDLEY-ELLIS(3)

(1) *The School of Electrical and Computer Engineering of Applied Studies*
Academy of Technical and Art Applied Studies
Belgrade, Serbia

(2) *The School of Electrical Engineering, Belgrade University*
Belgrade, Serbia; e-mail: dsumarac@etf.rs

(3) *The Centre for Wood Science and Technology, Edinburgh Napier University*
Edinburgh, United Kingdom; e-mail: D.Ridley-Ellis@napier.ac.uk

*Corresponding Author e-mail: filipp@viser.edu.rs

(*received October 19, 2021; accepted May 30, 2022*)

The aim of this research is to use a simple acoustic method of a very near field recording, which enables measurement and display of oscillation modes, to estimate the velocity of flexural waves, based on the wavelengths of standing waves measured on the sample. The paper analyses cases of 1D geometry, flexural waves that occur on a beam excited by an impulse. Measurements were conducted on two different samples: steel and a wooden beam of the same length. Due to the appearance of evanescent waves at the boundary regions, the distance between the nodes of standing waves that occur deviates from half the wavelength, which can be compensated using a correction factor. Cases of fixed and free boundary conditions were analysed. By quantifying how much the boundary conditions change the mode shape function, it can be predicted how the mode of oscillation changes if the boundary conditions change, which can also find application in musical acoustics and sound radiation analysis.

Keywords: mode shape function; flexural wave velocity; very near field.

1. Introduction

The mode shape function of the vibrating object could be calculated or simulated for different geometries and boundary conditions if the mechanical properties of the sample are known. Also, it can be done in a reverse way. Some information about material properties could be obtained by analysing a mode shape function. This concept is interesting for different reverse engineering problems in musical acoustics and also for non-destructive measurements when it is difficult to access material properties another way. This type of testing is especially important for wood as a material as its properties are sometimes hard to predict due to anisotropy, inhomogeneity, and their trend to change over time under the influence of all different factors like moisture and temperature. Whether it is a construction beam in a building or an old violin, non-invasive tests, if possible, are the best solution.

In musical acoustics plate patterns of violins and guitars have been the subject of study for many years starting from (Chladni, 1787) to new studies of (Gough, 2016) and (Woodhouse, 2014). Luthiers, in process of instrument making, optimize top plates response having in mind that when it is mounted on the instrument, mode shapes will change due to different boundary conditions and coupling with other body modes of an instrument. It is important to have a good

prediction of what will happen, and possibly make some measurements during this process, because when a plate is fixed to the body of the instrument there is nothing much to do to make changes in the instrument's response.

In this paper a procedure for estimation of flexural wave velocity of a beam by measuring mode shape function is presented. Additionally, in a broader context, this paper attempts to quantify how and where boundary conditions affect the change of mode shape function that occurs on the surface of vibrating objects. It allows us to adapt this measurement procedure for different boundary conditions and in situ cases.

Visualization of the oscillation modes of vibrating surface can be made by various optical methods, such as optical holography (Jansson *et al.*, 1970) or laser Doppler vibrometry (Bissinger, Oliver, 2007; Kalkert, Kayser, 2010; Gren *et al.*, 2006). A simple method presented in this paper, that proved to be good for this purpose without the need for special equipment, is the scanning of a sample in the Very Near Field (VNF) (Prezelj *et al.*, 2013; Pantelić, Prezelj, 2014; Keele, 1974). Placing the microphone in VNF, only a few millimeters above the vibrating surface allows recording of sound pressure level that is proportional to local surface velocity (de Bree *et al.*, 2004). The repeatability of VNF measurement is good because, in that zone, variations of sound pressure are small. Contrary to this, to do near-field measurements means small changes in the position of the microphone resulting in large differences in the recorded response. By using this technique it is possible to achieve good visualization of mode shapes (Pantelić *et al.*, 2020; Pantelić, Prezelj, 2014). The boundary of a VNF region is defined with the frequency and the distance of two adjacent nodes.

VNF recording is described in this paper, although the wave velocity estimation procedure can also be used in the case of other techniques for visualization of oscillation modes. By identifying the positions of the nodes of standing waves, the wavelength of flexural waves can be determined and the wave velocity could be calculated. Due to the complex nature of the analysed waves, the distance between nodes does not have to be equal to half the wavelength of propagating wave.

The governing wave equation for a vibrating uniform Euler–Bernoulli beam is the fourth-order equation (Meirovitch, 1986) so the solution of the equation includes propagating wave-like solutions – left and right going waves and also exponentially damped solutions – evanescent waves, well known and explained theoretically (Takiuti *et al.*, 2020; Diligent *et al.*, 2003; Ryden, Lowe, 2004).

In the mode shape equation, the trigonometric functions represent the propagating waves, and the hyperbolic functions represent the evanescent waves. Evanescent waves do not propagate through the medium, and they disappear quickly. Their influence is dominant near boundaries, so for higher-order modes, far from the edges, only propagating waves exist. Evanescent waves also could appear locally at excitation points in the case of forced vibrations or for the transient excitation (Graff, 1975).

As evanescent waves are superimposed with the propagating waves, the distance between adjacent nodes is not constant along the sample and it does not have to be equal to half of the wavelength of propagating waves, although right going and left going waves travel with constant velocity through the beam. For plates, mixing of these waves results in considerable curvature of the modal lines at the edges (Gough, 2007). The evanescent wave's influence on mode shape is a local phenomenon and it will be analysed, here, for the case of 1D geometry.

Flexural waves are dispersive, which comes directly from governing equation (Meirovitch, 1986). However, the Euler–Bernoulli theory applies only for slender beams – usually considered to be the case when the wavelength of a flexural wave is greater than about six times the thickness of the beam (Fahy, 1985). For the n-th mode of vibration, this criterion is approximately $\frac{L}{t} > n\pi$ where L and t are the length and thickness of the beam, respectively. This limitation of Euler–Bernoulli beam theory is due to the assumption that plane sections remain plane during bending. This is only true for pure bending but can be considered a negligible error for slender beams due to the small contribution of shear deformation to the behaviour. This is effectively the same as assuming the beam has infinite shear rigidity. This assumption, as well as that regarding rotational inertia, brings an anomaly in the results: the phase velocity increases without limit for increasing frequency (Graff, 1975). Other theories have a better prediction of wave velocity on high frequencies. Rayleigh's theory includes rotary-inertia effects (Rayleigh, 1945) and Timoshenko beam theory introduces shear modulus (Timoshenko, 1921). Those theories predict a plateau which the velocity reaches for high frequencies. Rayleigh's theory is seen to give bounded, but still too high, phase velocity for high frequencies. Euler–Bernoulli's theory is seen to agree with Timoshenko, and so-called "exact theory", in only a very limited range of low frequencies. For higher frequencies, or a thicker waveguide (beam or plate), the evanescent wave becomes propagating wave. The wavelengths become comparable with the cross-section and the simplified model is no longer valid (Takiuti *et al.*, 2020). Importantly for wood, most theoretical equations that include shear do so assuming the shear modulus (G) is simply related to the modulus of elasticity (E) by the Poisson's ratio, as is the case for isotropic materials. For wood, the role of G in flexural vibration needs to be considered explicitly for higher frequencies. This is because the wood has a relatively

low G compared to E, further complicated by the fact that the complex microstructure of wood means G and E can vary almost independently. This is much more complicated than the normally applied equation, but a relatively simple formulation of this, and an approach to the solution, has been provided in the wood science literature (Brancheriau, 2014). Even here, there is an assumption that the wood is homogenous and that the behaviour can be adequately described by the E along the grain and a single G for the parallel-perpendicular to the grain plane.

Considering the frequency range examined in this study, all theories predict that the wave velocity increases with the square root of the frequency. Modes of a wooden beam have been measured in VNF up to 12th order. For those frequencies using the simpler Bernoulli–Euler theory is justified as the case of the slender beam. Besides the analysed wooden beam, a steel beam of the same length is also measured to justify the use of the correction factor that will be introduced in this paper. Measurements on the steel beam will exclude the influence of anisotropy and inhomogeneity which appear in the case of wood.

2. Analytical solution and correction for wavelength estimation

Mode shape functions of a vibrating beam of length L for different boundary conditions are presented in Fig. 1. The analytical solution of a mode shape function of the first three modes for free-free and fixed-fixed boundary conditions and second, third and fourth mode for cantilever beam are presented with a solid line on the graph. The first mode for the cantilever beam is intentionally omitted because it does not have any standing wave nodes. Mode shapes in the case when the hyperbolic components are removed from the mode shape function are presented with a dashed line. The distance between the nodes formed with dashed lines corresponds to half the wavelength of the propagating component but in reality, that distance becomes changed (the case of the solid line) due to the superposition with evanescent waves. There is a shortening on the side where there are the free boundary conditions and increasing on the side where fixed boundary conditions are.

The effect disappears moving away from the edges of the sample so the dashed line and solid line match each other half the wavelength from the edge. The scenario is the same for higher modes – the difference exists only half the wavelength from the edge. In the case of modes greater order than three, it is enough to select two nodes away from the boundary and the distance between them will correspond to half the wavelength of the propagating wave. This can be applied to some extent in the case of the third mode for free-free and fixed-fixed boundary conditions and the fourth for cantilever beam because the differences between these two curves in the middle of the sample

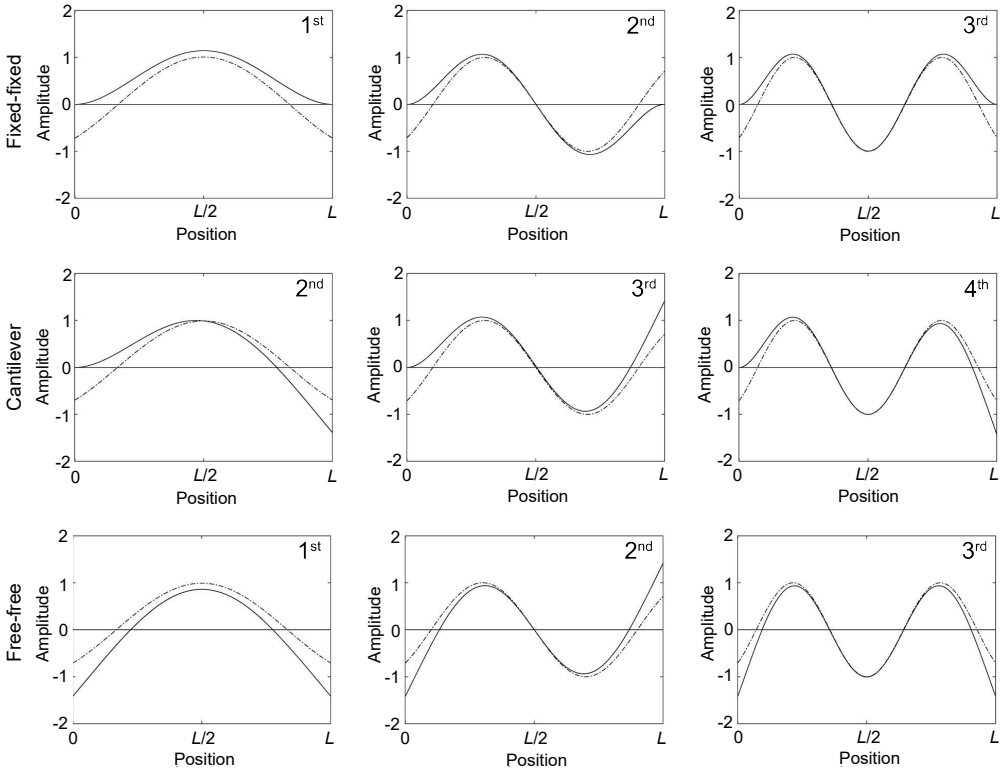

Fig. 1. Mode functions (full line) and mode functions without hyperbolic component (dashed line) for different boundary conditions: fixed-fixed (1st, 2nd, 3rd mode), cantilever beam (2nd, 3rd, 4th mode), free-free (1st, 2nd, 3rd mode).

Table 1. Relationship of the distance between nodes d and half of the wavelength $\lambda/2$ for the fixed side of the sample (total length of the sample is $L = 1$).

b.c.	Fixed-fixed				Cantilever beam (fixed side)			
No.	1	2	3	4	1	2	3	4
$a \cdot L$	4.73	7.853	10.996	14.137	1.875	4.694	7.855	10.996
d	1	0.5	0.3584	0.2788	/	0.7835	0.5035	0.3583
$\lambda/2$	0.6642	0.4001	0.2857	0.2222	/	0.6693	0.3999	0.2857
C_λ	0.6642	0.8001	0.7971	0.7972	/	0.8543	0.7943	0.7973

Table 2. Relationship of the distance between nodes d and half of the wavelength $\lambda/2$ for free side of the sample (total length of the sample is $L = 1$).

b.c.	Free-free				Cantilever beam (free side)			
No.	1	2	3	4	1	2	3	4
$a \cdot L$	4.73	7.853	10.996	14.137	1.875	4.694	7.855	10.996
d	0.5516	0.3679	0.2614	0.2033	/	0.7835	0.3641	0.2615
$\lambda/2$	0.6642	0.4001	0.2857	0.2222	/	0.6693	0.3999	0.2857
C_λ	1.2041	1.0874	1.0932	1.0929	/	0.8543	1.0984	1.0927

are very small (about 1.4%). In the case of the lowest mode for all boundary conditions, evanescent waves are present along the entire length of the sample, so the measured distance between the nodes deviates significantly from half the wavelength of the propagating wave. To overcome those differences in measurement procedure correction factor can be introduced as:

$$C_\lambda = \frac{\lambda}{2d}, \tag{1}$$

where d is the distance between nods and λ wavelength. For Euler–Bernoulli beams correction factor C_λ depends only on the boundary conditions and the mode number and it can be numerically calculated for every case of interest by using the analytical solution of the mode shape function. Mode shape function zeroes, with and without hyperbolic components, are numerically calculated assuming that the length of the sample is 1. The calculation is done for all resonances, defined by the value of wavenumber a, which can be found in the literature (Meirovitch, 1986). Obtained values are given in Table 1 for the fixed side of a sample, and in Table 2 for the free side. The distance between zeroes for the regular mode is denoted by d, while the distance in the case when the hyperbolic components are excluded from the function is denoted by $\lambda/2$. The ratio between the values of these distances C_λ is also shown in Tables 1 and 2.

Theoretically, coefficient C_λ does not depend on the dimensions and mechanical properties of the beam, so by knowing its values, half the wavelength of the propagating wave can be estimated by multiplying the measured distance between nodes d by this coefficient. For all modes of a higher order than 4, the coefficient C_λ does not differ much from the values for the 4th mode.

3. Experimental verification

3.1. Measurement procedure

In order to test the conclusions made in the previous paragraph, the following experiment was performed in which beams were analysed in free boundary conditions.

The experimental setup is shown in Fig. 2. The sample is placed on elastic bands to achieve free-free boundary conditions. During the measurement, the specimen was manually excited by impulse (hammer) consistently at the same point. In addition to the sample on elastic bands, this setup employs two microphones with a 10 mm membrane diameter. The moveable microphone M1 is set in a VNF at a distance of several millimeters from the sample. Response at measurement points, 5 mm one from another, along the length of the sample was recorded with this microphone. The non-uniformity of the sample excitation for each measurement point is compensated by the referent microphone M2. This microphone is positioned in

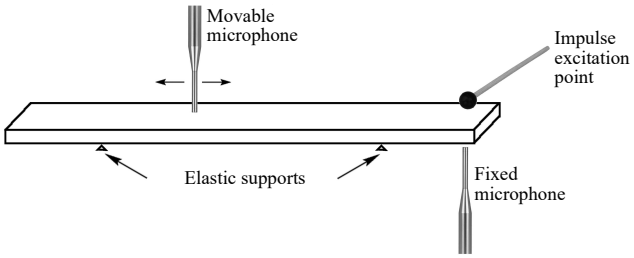

Fig. 2. Experimental setup – beam in free-free boundary conditions.

VNF at one fixed point, and it does not move through all measurements. Its role is to register variations in different levels of sound pressure due to a non-uniform hammer impact. The signals recorded with the M1 microphone are increased or decreased according to variations of the signal level recorded with the M2 microphone.

3.2. Flexural wave velocity estimation of a wooden beam

The properties of the analysed wooden beam are given in Table 3. Values of modulus of elasticity are approximated using the standard acoustical method of E approximation, defined by standard procedures (ASTM E1875-13, 2013; ASTM E1876-15, 2015). Sample mass m was measured, and density ρ was calculated.

The internal structure of the analysed wooden beam is oriented in the way that the longest dimension of the sample matches the longitudinal direction of the wood grain. Impulse response was recorded at 92 measuring points and for every point, FFT is calculated. From the recorded signal spectrum resonant frequencies of a beam are identified and they are presented in Table 4. By calculating FFT for all measurement points sound pressure levels above the whole surface of the sample can be displayed for any frequency in the analysed range. Figure 3 shows the dependence of the sound pressure level from the measuring position for the 1st, 2nd, 3rd, and 8th mode of the beam.

Velocity estimation was made for frequencies of twelve resonant minor axis flexural modes appearing on the beam by measuring a wavelength from a mode shape function like those presented in Fig. 3. Wavelengths can be measured not only for the resonance

Table 3. Wooden beam material properties.

Material	Mass [g]	Length [mm]	Thickness [mm]	Width [mm]	ρ [kg/m^3]	E [GPa]
Wood	23.46	456	3.5	19.8	742.4	15.6

Table 4. Node distance d, half wavelength $\lambda/2$, and estimated flexural wave velocity v for the wooden beam in free-free boundary conditions.

f [Hz]	79	217	425	700	1036	1451	1912	2447	3038	3684	4409	5118
d [m]	0.2550	0.1675	0.1225	0.1025	0.0850	0.0700	0.0550	0.0525	0.0475	0.0450	0.0400	0.0375
$\lambda/2$ [m]	0.307	0.182	0.1225	0.1025	0.0850	0.0700	0.0550	0.0525	0.0475	0.0450	0.0400	0.0375
v [m/s]	48.5	79.0	104.1	143.5	176.1	203.1	210.3	256.9	288.6	331.6	352.7	383.9

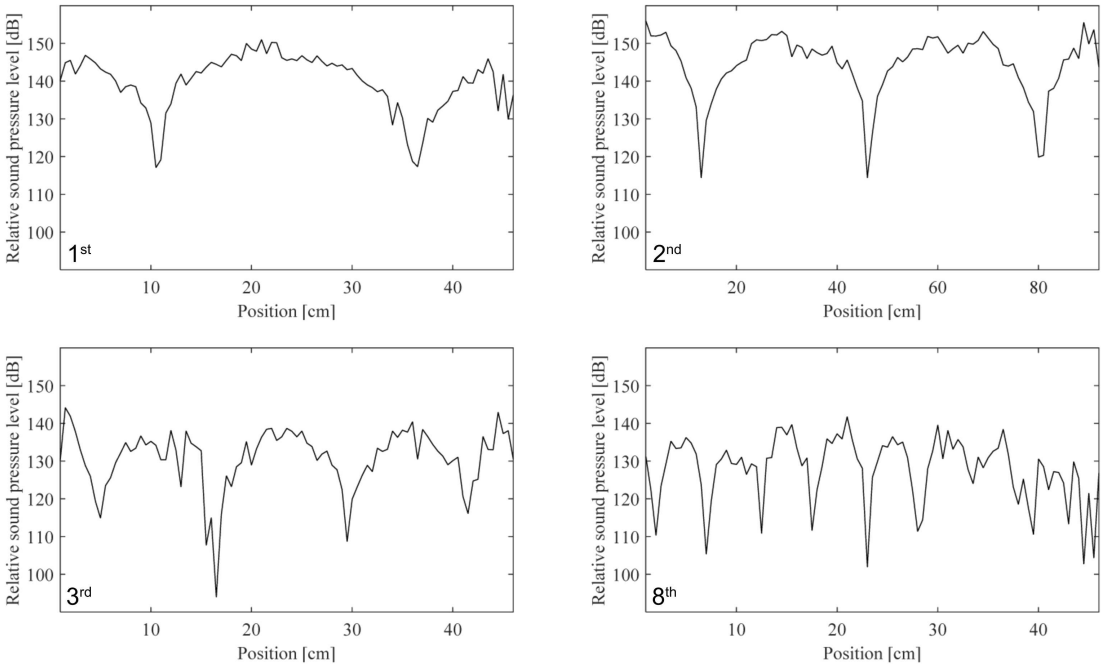

Fig. 3. Dependence of the sound pressure level from the measuring position for the 1st, 2nd, 3rd, and 8th mode of the beam (79 Hz, 217 Hz, 425 Hz, and 2447 Hz, respectively).

frequencies but also for any frequencies in the analysed range. However, the easiest way to see the minimum is on the resonant frequency, so these cases are taken into account. As the distance between the two measuring positions during the sample scan was 0.5 cm, the measured node position can deviate from its real value, and this error becomes more significant at higher frequencies where the wavelengths are shorter. For higher frequencies, this could be overcome by measuring distance, not between adjacent nodes but far ones, and dividing value with the appropriate number (for example see 8th mode on Fig. 3 where several "hills" could be identified). In Table 4 measured distances d are shown with their corresponding frequencies.

If it is assumed that the distance between the two adjacent minima corresponds to half the wavelength of propagating waves, which is true for positions far from edges of the sample, it is possible to estimate flexural waves velocity. As it was mentioned before, evanescent waves, which appear near edges, are superimposed with propagating waves which result in shifting node positions in this region. For modes higher than order two it is possible to choose two adjacent minimums in regions far from the edge, but for the 1st and 2nd mode, there are no nodes out of this region. This is why the node distance for this case does not match half the wavelength of a propagating wave. To correct this difference the correction factor that was defined in Table 2 (free-free boundary conditions) is applied for the two lowest modes. Values for $\lambda/2$ are equal to d except for 1st and 2nd mode where the correction is applied.

By multiplying wavelength with frequency velocity values are calculated for the first 12 modes. The values of wave velocity depending on the frequency are shown in Fig. 4a. These waves are dispersive so the velocity of the flexural waves is frequency dependent. More precisely, the velocity is proportional to the root of the frequency. For this reason, squared root values of frequency are given on the x-axis in Fig. 4a.

The estimated velocity values coincide with the theoretical expectations in the analysed frequency region. Through the twelve points in which velocity values are estimated, a regression line passing through (0.0) point is calculated and it appears in Fig. 4a. The equation of this line is also shown in Fig. 4a. The value of the determination coefficient for this trend line is $R^2 = 0.9948$. The measured velocity values deviate more from the trend line at high frequencies, which is expected due to a larger measurement error in this band. Combined uncertainty for all measurement positions is calculated and presented in Fig. 4a.

For low frequencies, an error is smaller and those measurements are most relevant. That's why it is important to use the first two modes in the calculation. By using a correction factor for the first two modes good agreement with theoretical expectations was achieved and estimated values for low frequency velocity match the regression line. In Fig. 4b results are presented only for a low frequency region. Values marked with crosses are cases when the correction factor was not applied to measured data.

3.3. Flexural wave velocity estimation of a steel beam

Measurements are also made for the steel beam of the same length. The properties of the analysed sample are given in Table 5. Values of modulus of elasticity are approximated by standard procedures (ASTM E1875-13, 2013; ASTM E1876-15, 2015). Sample mass m was measured, and density ρ was calculated.

The same procedure for mode visualization is applied as in the case of wooden beam, and results are presented in Table 6 and graphically in Fig. 5.

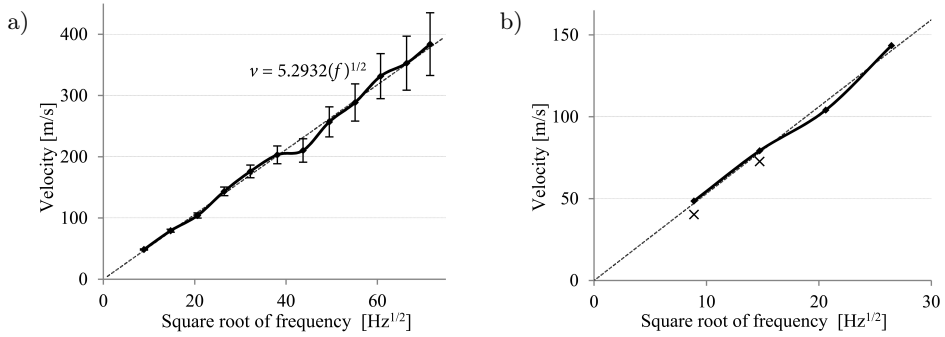

Fig. 4. The velocity of flexural waves estimation for wooden beam in free-free boundary conditions: a) full range with measurement uncertainty, b) matching the trend line for low frequency range – with correction (small squares) and without correction (crosses).

Table 5. Steel beam material properties.

Material	Mass [g]	Length [mm]	Thickness [mm]	Width [mm]	ρ [kg/m^3]	E [GPa]
Metal	142	456	2	20	7785.1	191.2

Table 6. Node distance d, half wavelength $\lambda/2$, and estimated flexural wave velocity v for the steel beam in free-free boundary conditions.

f [Hz]	49	137	268	442	662	924	1231	1581	1976	2413	2899	3422
d [m]	0.2550	0.1650	0.1300	0.1050	0.0850	0.0700	0.0600	0.0550	0.0475	0.0433	0.0400	0.03875
$\lambda/2$ [m]	0.3070	0.1794	0.1300	0.1050	0.0850	0.0700	0.0600	0.0550	0.0475	0.0433	0.0400	0.03875
v [m/s]	30.1	49.2	69.7	92.8	112.5	129.4	147.7	173.9	187.7	209.1	231.9	265.2

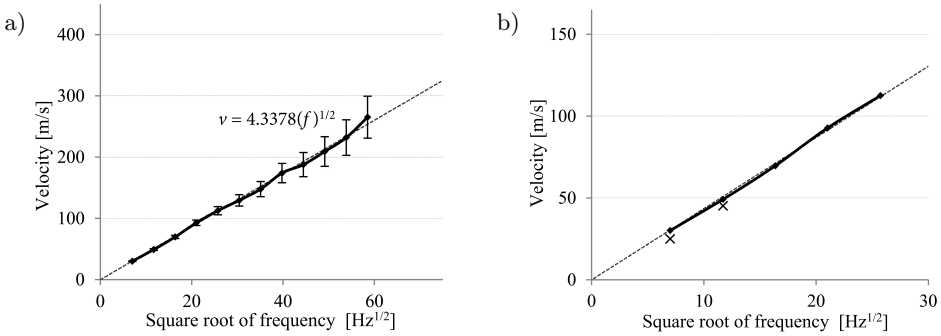

Fig. 5. The velocity of flexural waves estimation for steel beam in free-free boundary conditions: a) full range with measurement uncertainty; b) matching the trend line for low frequency range – with correction (small squares) and without correction (crosses).

The value of the determination coefficient of a trend line for steel beam measurement in Fig. 5a is R^2 = 0.9965. As expected, in the case of steel beam agreement with theoretical expectations is even better than in the case of wood. Estimated values for low frequency velocity match the regression line, while values without correction applied, marked with crosses in Fig. 5b, lie under the regression line.

4. Conclusion

This paper describes a procedure for estimating the velocity of flexural waves that occur in beams based on the wavelengths of standing waves measured with simple instrumentation. The wavelengths were determined based on the mode shapes obtained by measuring the sound pressure with a microphone in a very near field a few millimeters from the beam. At high frequencies, an error in wavelength estimation occurs due to the low scanning resolution of the sample as the response is recorded in 92 points with a distance of 0.5 cm. Reducing this distance can improve the results but extends the time required for this type of measurement. For higher frequencies, if possible, this could be overcome by measuring distance, not between adjacent nodes but far ones, and dividing value with the appropriate number to get one wavelength. Often it is hard to find a good minimum for high frequency so this approach is not systematically included in the calculation of combined uncertainty for this measurement. Besides the dimensions of the microphone membrane compared with the wavelength, the reasons for bad readings of sound pressure for high frequencies are due to the appearance of other modes of oscillation in that frequency region. This especially stands for torsional waves. In the FEM model of the analysed steel beam in free-free boundary conditions, torsional modes start to occur from 663 Hz (in used numerical model Poisson's ratio was 0.28). For wood samples, it is harder to predict torsional mode frequencies due to complicated wood structure but they are expected in a similar frequency range. This could explain deviations in estimated values of velocity starting from the 7th mode in Fig. 3.

For low frequencies, the distance between the nodes is not equal to half the wavelength due to the existence of evanescent waves at the edges of the sample. By correcting the measured values using the correction factor which is proposed in this paper, the value of the wavelength can be reached, which was done for the lowest two modes. The measurement error is smaller in this region (combined uncertainty is about 2% for 1st mode) compared to the error for high frequencies (13.3% for 12th mode) so first modes are most important for this type of measurement, which increases the importance of applied wavelength correction. The influence of evanescent waves on the estimation of the wavelength for higher frequencies can be avoided if the distance between the nodes is measured at positions that are half the wavelength away from the sample boundaries.

References

1. ASTM E1875-13 (2013), *Standard Test Method for Dynamic Young's Modulus, Shear Modulus, and Poisson's*

Ratio by Sonic Resonance, ASTM International, doi: 10.1520/E1875-13.

2. ASTM E1876-15 (2015), *Standard Test Method for Dynamic Young's Modulus, Shear Modulus, and Poisson's Ratio by Impulse Excitation of Vibration*, ASTM International, doi: 10.1520/E1876-21.
3. Bissinger G., Oliver D. (2007), 3-D laser vibrometry on legendary old Italian violins, *Sound and Vibration*, **3**(7): 10–14.
4. Brancheriau L. (2014), An alternative solution for the determination of elastic parameters in free–free flexural vibration of a Timoshenko beam, *Wood Science and Technology*, **48**: 1269–1279, doi: 10.1007/s00226-014-0672-x.
5. Chladni E.F.F. (1787), *Discoveries on the theory of sound*, [in German: *Entdeckungen über die Theorie des Klanges*], Leipzig: bey Weidmanns Erben und Reich, doi: 10.3931/e-rara-4235.
6. de Bree H.-E., Svetovoy V., Raangs R., Visser R. (2004), The very near field, theory, simulations and measurements of sound pressure and particle velocity in the very near field, [in:] *Proceedings of the 11th International Congress on Sound and Vibration*, pp. 1–8.
7. Diligent O., Lowe M.J.S., Le Clézio E., Castings M., Hosten B. (2003), Prediction and measurement of evanescent Lamb modes at the free end of a plate when the fundamental antisymmetric mode A_0 is incident, *The Journal of the Acoustical Society of America*, **113**(6): 3032–3042, doi: 10.1121/1.1568758.
8. Fahy F. (1985), *Sound and Structural Vibration, Radiation, Transmission and Response*, Academic Press Inc., New York.
9. Gough C. (2007), The violin: Chladni patterns, plates, shells and sounds, *The European Physical Journal Special Topics*, **145**: 77–101, doi: 10.1140/epjst/e2007-00149-0.
10. Gough C. (2016), Violin acoustics, *Acoustics Today*, **12**(2): 22–30.
11. Graff K.F. (1975), *Wave Motion in Elastic Solids*, Ohio State University Press.
12. Gren P., Tatar K., Granström J., Molin N.-E., Jansson E. V. (2006), Laser vibrometry measurements of vibration and sound fields of a bowed violin, *Measurement Science and Technology*, **17**(4): 635–644, doi: 10.1088/0957-0233/17/4/005.
13. Jansson E., Molin N.-E., Sundin H. (1970), Resonances of a violin body studied by hologram interferometry and acoustical methods, *Physica Scripta*, **2**(6): 243–256, doi: 10.1088/0031-8949/2/6/002.
14. Kalkert C., Kayser J. (2010), *Laser Doppler Velocimetry*, Biophysics Laboratory, University of California, San Diego.
15. Keele D.E. (1974), Low-frequency loudspeaker assessment by nearfield sound-pressure measurement, *Journal of the Audio Engineering Society*, **22**(3): 154–162.
16. Meirovitch L. (1986), *Elements of Vibration Analysis*, McGraw-Hill College.
17. Pantelić F., Mijić M., Šumarac Pavlović D., Ridley-Ellis D., Dudeš D. (2020), Analysis of a wooden specimen's mechanical properties through acoustic measurements in the very near field, *The Journal of the Acoustical Society of* America, **147**(4): EL320-EL325, doi: 10.1121/10.0001030.
18. Pantelić F., Prezelj J. (2014), Hair tension influence on the vibroacoustic properties of the double bass bow, *The Journal of the Acoustical Society of America*, **136**(4): EL288–EL294, doi: 10.1121/1.4896408.
19. Pantelić F., Ridley-Ellis D., Mijić M., Šumarac Pavlović D. (2017), Monitoring changes in wood properties using Very Near Field sound pressure scanning, [in:] *4th Annual Conference COST FP1302 WoodMusICK*, Brussels, Belgium.
20. Prezelj J., Lipar P., Belšak A., Čudina M. (2013), On acoustic very near field measurements, *Mechanical Systems and Signal Processing*, **40**(1): 194–207, doi: 10.1016/j.ymssp.2013.05.008.
21. Rayleigh J.W.S. (1945), *The Theory of Sound*, Vol. I–II, Dover Publications, New York.
22. Ryden N., Lowe M.J.S (2004), Guided wave propagation in three-layer pavement structures, *The Journal of the Acoustical Society of America*, **116**(5): 2902–2913, doi: 10.1121/1.18082231.
23. Takiuti B.E., Manconi E., Brennan M.J., Lopes Jr. V. (2020), Wave scattering from discontinuities related to corrosion-like damage in one-dimensional waveguides, *Journal of the Brazilian Society of Mechanical Sciences and Engineering*, **42**: 521, doi: 10.1007/s40430-020-02574-1.
24. Timoshenko S.P. (1921), On the correction for shear of the differential equation for transverse vibrations of prismatic bars, *The London, Edinburgh, and Dublin Philosophical Magazine and Journal of Science*, **41**(245): 744–746, doi: 10.1080/14786442108636264.
25. Woodhouse J. (2014), The acoustics of the violin: a review, *Reports on Progress in Physics*, **77**(11): 115901.